

École doctorale n° 364 : Sciences Fondamentales et Appliquées

Doctorat ParisTech

THÈSE

pour obtenir le grade de docteur délivré par

l'École Nationale Supérieure des Mines de Paris

Spécialité doctorale “Science et Génie des Matériaux”

présentée et soutenue publiquement par

Ali SAAD

le xx mai 2015

NUMERICAL MODELLING OF MACROSEGREGATION INDUCED BY SOLIDIFICATION SHRINKAGE IN A LEVEL SET APPROACH

Directeurs de thèse: **Michel BELLET**
Charles-André GANDIN

Jury

M. Blablabla,	Professeur, MINES ParisTech	Rapporteur
M. Blablabla,	Professeur, Arts Et Métiers ParisTech	Rapporteur
M. Blablabla,	Chargé de recherche, ENS Cachan	Examinateur
M. Blablabla,	Danseuse, en freelance	Examinateur
M. Blablabla,	Ingénieur, MIT	Examinateur

T
H
E
S
S

Contents

1 General Introduction	1
1.1 Casting defects	2
1.2 Macrosegregation	3
1.2.1 Causes	4
1.2.2 Types	5
1.3 Industrial Worries	7
1.4 Project context and objectives	8
1.4.1 Context	8
1.4.2 Objectives and outline	9
2 Modelling Review	11
2.1 Modelling macrosegregation	12
2.1.1 Dendritic growth	12
2.1.2 Mush permeability	12
2.1.3 Microsegregation	13
2.1.4 Macroscopic solidification model: monodomain	16
2.2 Eulerian and Lagrangian motion description	20
2.2.1 Overview	20
2.2.2 Interface capturing	21
2.3 Solidification models with level set	22
2.4 The level set method	22
2.4.1 Diffuse interface	23
2.4.2 Mixing Laws	24
2.4.3 Transport and regularisation	26
2.4.4 Interface Remeshing	28
Bibliography	29

Contents

Acronym	Standing for
ALE	Arbitrary Lagrangian-Eulerian
CCEMLCC	Chill Cooling for the Electro-Magnetic Levitator in relation with Continuous Casting of steel
CEMEF	Center for Material Forming
DLR	Deutsches Zentrum für Luft- und Raumfahrt
EML	Electromagnetic levitation
ESA	European Space Agency
FEM	Finite Element Method
ISS	International Space Station
IWT	Institut für Werkstofftechnik
LHS	Left Hand Side
MAC	Marker-and-cell
PF	Phase field
RHS	Right Hand Side
RUB	Ruhr Universität Bochum
RVE	Representative Elementary Volume
VOF	Volume Of Fluid

Contents

Chapter 1

General Introduction

Macrosegregation is a very known defect to metallurgical processes. Despite a great evolution achieved by active research during the last 60 years, it remains partially understood. Macrosegregation is often the consequence of several factors at the scale of a casting, all related to *microsegregation* happening at the scale of dendrites. Today, research in metallurgy focuses on a deeper understanding of such a connection between the different physical scales. Solidification is not only a phase change, but also a complex transformation involving small scales like nucleation, medium scales like grains growth and large scales like convection in the melt. From the nucleation theory to the mechanical behavior of metals, intricate phenomena combine to form defects in the final product. This has been seen in casting processes, such as continuous casting (fig. 1.1) and ingot casting. Surface and volume porosity, hot tearing and composition heterogeneity are known defects to the casting community. After a brief introduction of these defects, macrosegregation will be the focus of this dissertation.



Fig. 1.1 – Main steps in a continuous casting plant

1.1 Casting defects

Undesired effects are inevitable in any industrial process. More importantly, a lot of defects in the casting industry can be disastrous in some situations where the cast product is not serviceable and hence rejected. This leads to a systematic product recycling, i.e. the product is ditched to be reheated, remelted and then cast again. From an economic point view, the operation is expensive timewise and profitwise. Understanding and preventing defects when possible, is thus crucial in the casting industry. We focus hereafter on the main encountered defects.

Hot tearing

This defect, also denoted solidification cracking or hot cracking, occurs in the mushy zone at high solid fractions when a failure or crack appears at specific locations, the hot spots. The temperature range in which the steel is vulnerable to hot tearing is known as the brittleness temperature range (BTR). It corresponds to solid fractions greater than 90%, with the liquid phase forming a discontinuous film. Many factors can cause the failure, but the main origin is a lack of liquid feeding required to compensate for the solidification shrinkage, in the presence of thermal stresses in the mushy region. Therefore, a crack initiates then propagates in the casting, as shown in [fig. 1.2](#).



Fig. 1.2 – Crack in an aluminium slab

Porosity

Porosity is a void defect formed inside the casting or at the outer surface. It may attributed to two different factors. Firstly, we speak of *shrinkage porosity*, when a void forms as a result of density differences between the interdendritic liquid and solid network, the latter being denser than the former ([figs. 1.3c and 1.3d](#)). It is basically, the same reason that initiates hot cracks. The second factor is the presence of dissolved gaseous phases in the melt ([figs. 1.3a and 1.3b](#)). According to [Dantzig et al. \[2009\]](#), these gases may be initially in the melt, or created by the reaction between the metal and water found in the air or at trapped in grooves at the moulds surface. If the decreasing temperature and pressure drop in the liquid are large

enough, the latter becomes supersaturated. Consequently, the nucleation of gaseous phase is triggered (just like when you open a cold bottle of coca-cola is opened!).



Fig. 1.3 – Examples of porosity in casting and welding

Freckles or segregated channels

The origin of this defect is a combined effect of microsegregation and buoyancy forces. Upon solidification, solid forms while rejecting some solute in the liquid due to partitioning (steels have a partition coefficient less than unity). When segregated solute is the lighter species, an increasing concentration in the liquid phase produces a solutal driving force inside the mushy zone, generating unstable convection currents, with "plume" shapes as often reported in the literature [Sarazin et al. 1992; Schneider et al. 1997; Shevchenko et al. 2013]. When temperature gradient is an additional force of convection, the latter is hence qualified as "thermosolutal".

1.2 Macrosegregation

Macrosegregation generally stems from a solubility difference between a liquid phase and one or more solid phases, along with a relative velocity between these phases. While the former is responsible for local solute enrichment or depletion, the latter will propagate the composition heterogeneity on a scale much larger than just a few dendrites. This is why macrosegregation could be observed on the scale of a casting, up to several meters in length.

While microsegregation can be healed by annealing the alloy to speed up the diffusion process and allow homogenization, heterogeneities spanning on larger distances cannot be treated after solidification. It is obvious that macrosegregation is irreversible defect. Failure to prevent it may lead to a substantial decline in the alloy's mechanical behavior, hence its serviceability.

1.2.1 Causes

Four main factors can (simultaneously) cause fluid flow leading to macrosegregation:

Liquid dynamics

During solidification, thermal and solutal gradients result in density gradients in the liquid phase:

$$\rho^l = \rho_{\text{ref}}(1 - \beta_T(T - T_{\text{ref}}) - \sum_i \beta_{w_i^l}(w_i^l - \langle w_i \rangle_{\text{ref}}^l)) \quad (1.1a)$$

$$\vec{\nabla} \rho^l = -\rho_{\text{ref}}(\beta_T \vec{\nabla} T + \sum_i \beta_{w_i^l} \vec{\nabla} w_i^l) \quad (1.1b)$$

In eq. (1.1a), density is assumed to vary linearly with temperature and phase composition for each chemical species (index i). The slopes defining such variations are respectively the thermal expansion coefficient β_T and solutal expansion coefficient $\beta_{w_i^l}$, given by [Kohler 2008]:

$$\beta_T = -\frac{1}{\rho_{\text{ref}}} \left(\frac{\partial \rho^l}{\partial T} \right) \quad (1.2a)$$

$$\beta_{w_i^l} = -\frac{1}{\rho_{\text{ref}}} \left(\frac{\partial \rho^l}{\partial w_i^l} \right) \quad (1.2b)$$

The linear fit assumes also that the density takes a reference value, ρ_{ref} , when temperature and liquid composition reach reference values, respectively T_{ref} and $\langle w_i \rangle_{\text{ref}}^l$. However, in some situations, a suitable thermodynamic database providing accurate density values is far better than a linear fit, especially in the current context of macrosegregation. Such possibility will be discussed later in the manuscript (cf. SECTION TODO)

In the presence of gravity, the density gradient in eq. (1.1b), causes thermosolutal convection in the liquid bulk and a subsequent macrosegregation.

Solidification shrinkage

Solid alloys have a greater density than the liquid phase ($\rho^s > \rho^l$), thus occupy less volume. Upon solidification, the liquid moves towards the solidification front to compensate for the volume difference caused by the phase change, as well as the thermal contraction. When macrosegregation is triggered by solidification shrinkage, we speak of *inverse segregation*. Theoretically, if solute mass is conserved, a decreasing volume results in a positive segregation. Shrinkage deforms the outer surface of a solidifying alloy, causing positive macrosegregation.

While one would naturally expect negative macrosegregation in areas where solidification begins and positive inside the alloy, shrinkage promotes the opposite phenomenon, hence the term *inverse segregation*. In contrast to liquid convection, shrinkage flow may cause macrosegregation even without gravity.

Movement of equiaxed grains

Equiaxed grains can grow in the liquid bulk where thermal gradients are weak, or in the presence of inoculants. Consequently, they are transported by the flow (floating or sedimenting, depending on their density [Beckermann 2002]) which leads to negative macrosegregation in their final position.

Solid deformation

Stresses of thermal and mechanical nature are always found in casting processes (e.g. bulging between rolls in continuous casting). Deformation of the semi-solid in the mushy zone causes a relative solid-liquid flow in the inward (tensile stresses) or outward (compressive stresses) direction, causing macrosegregation.

1.2.2 Types

In continuous casting

The semi-solid billet is carried through a series of rolls that exert a radial force to straighten it and get it to its horizontal position. As the mushy part of a slab enters through these rolls, interdendritic liquid is expelled backwards, i.e. regions with lower solid fraction. Since the boundaries solidify earlier than the centre, the enriched liquid accumulates halfway in thickness, forming a centreline macrosegregation as shown in fig. 1.4. Other types of segregates (channels, A-segregates ...) can also be found but remain more specific to ingot casting.

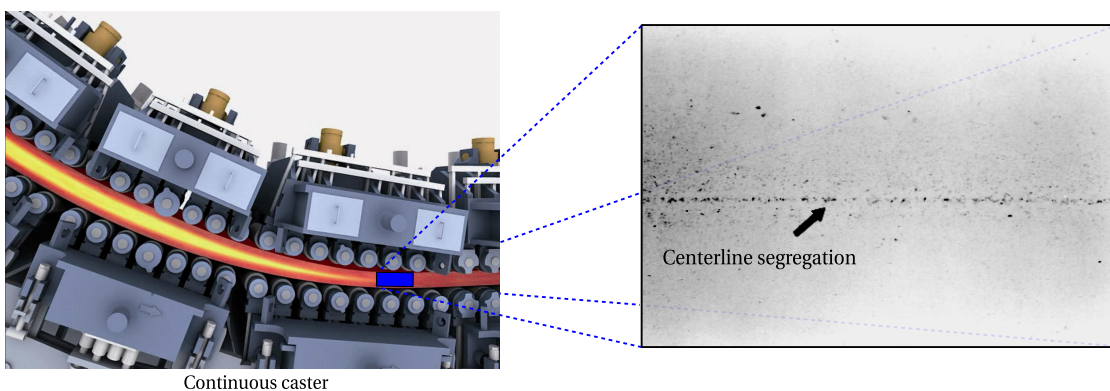


Fig. 1.4 – Centreline segregation in a steel slab [Beckermann 2002]

In ingot casting

A variety of segregation patterns can be encountered in heavy ingots:

- the lower part is characterized by a negative segregation cone promoted by the sedimentation of equiaxed crystals,
- positive segregation channels, known as A-segregates, form along the columnar dendritic zones, close to the vertical contact with the mould,
- positive V-segregates can be identified in the centre of the ingot,
- a positive macrosegregation in the upper zone where the last liquid solidifies, the so-called "hot-top", caused by solidification shrinkage (inverse segregation) and thermosolutal buoyancy forces.

Combeau et al. [2009] state that A-segregates and V-segregates formation is mainly attributed to local flow phenomena. As such, their scale is finer than macrosegregation, hence called "mesosegregates".



Fig. 1.5 – Sulphur print (left) of a 65-ton steel ingot [Lesoult 2005] showing various patterns (right) of macrosegregation [Flemings 1974]

In investment casting

This process is widely used to cast single-crystal (SC) alloys for turbines and other applications that require excellent mechanical behavior [Giamei et al. 1970]. During directional solidification, thermosolutal forces thrust segregated species outside of the mushy zone into the liquid bulk. The segregation scale ranges from a few dendrites to a few hundreds of them, hence forming "long and narrow trails" (fig. 1.6a) as described by Felicelli et al. [1991]. Freckles are frequently formed by small equiaxed grains (fig. 1.6b), probably caused by a uniform temperature gradient that settles as the channels become richer in solute. They can be observed on the ingot's surface, as well as in the volume.

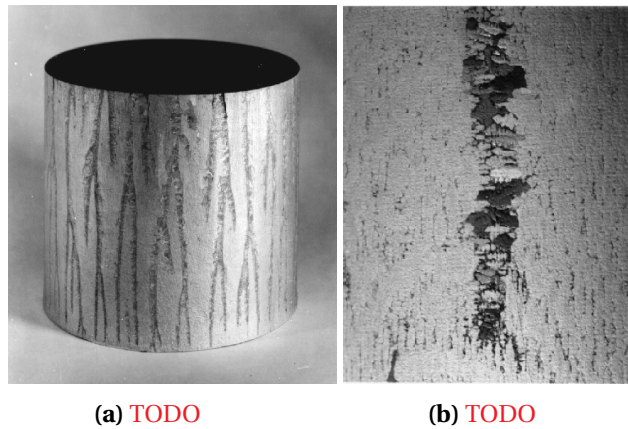


Fig. 1.6 – Freckles in directional casting of nickel-base superalloys

1.3 Industrial Worries

Steel production has continuously increased over the years to meet the industrial needs. [Figure 1.7](#) shows this increase between 1980 and 2013 with a clear dominance of the Chinese production. Quality constraints have also increased where specific grades of steel are needed in critical applications such as mega-structures in construction and heavy machinery. Therefore, alloys with defects are considered vulnerable and should be avoided as much as possible during the casting process. As such, steelmakers have been investing in research, with the aim of understanding better the phenomena leading to casting problems, and improve the processes when possible.



Fig. 1.7 – Evolution curves of crude steel worldwide production from 1980 to 2013

Simulation software dedicated to alloy casting is one of the main research investments undertaken by steelmakers. These tools coming from academic research are actively used to optimize the process. However, few are the tools that take into account the casting environ-

Chapter 1. General Introduction

ment. For instance, the continuous casting process, in [fig. 1.1](#), is a chain process where the last steps involve rolls, water sprays and other components. A dedicated software is one that can provide the geometric requirements with suitable meshing capabilities, as well as respond to metallurgical and mechanical requirements, mainly:

- handling moulds and their interaction with the alloy (thermal resistances ...)
- handling alloy filling and predicting velocity in the liquid and mushy zone
- handling thermomechanical stresses in the solid
- handling multicomponent alloys and predicting macrosegregation
- handling finite solute diffusion in solid phases
- handling real alloy properties (not just constant thermophysical/thermomechanical properties)

1.4 Project context and objectives

1.4.1 Context

The European Space Agency (ESA) has been actively committed, since its foundation in 1975, in the research field. Its covers not only exclusive space applications, but also fundamental science like solidification. This thesis takes part of the ESA project entitled *CCEMLCC*, abbreviating "Chill Cooling for the Electro-Magnetic Levitator in relation with Continuous Casting of steel". The three-year contract from 2011 to late 2014 denoted *CCEMLCC II*, was preceded by an initial project phase, *CCEMLCC I*, from 2007 to 2009. The main focus is studying containerless solidification of steel under microgravity conditions. A chill plate is later used to extract heat from the alloy, simulating the contact effect with a mould in continuous casting or ingot casting. A partnership of 7 industrial and academic entities was formed in *CCEMLCC II*. A brief summary of each partner's commitment:

Academic partners

- CEMEF (France): numerical modelling of microgravity chill cooling experiments
- DLR (German Aerospace Centre) and RUB university (Germany): preparation of a chill cooling device for electromagnetic levitation (EML), microgravity testing and investigation of growth kinetics in chill-cooled and undercooled steel alloys
- University of Alberta (Canada): impulse atomization of the D2 tool steel
- University of Bremen - IWT institute (Germany): study of melt solidification in atomization processing

Industrial partners

- ARCELORMITTAL (France): elaboration of a series of steel grades used in microgravity and ground studies

- METSO Minerals Inc. (Finland): material production with D2 tool steel for spray forming
- TRANSVALOR (France): development and marketing of casting simulation software *Thercast[®]*

CEMEF, as an academic partner, contributed to the work by proposing numerical models in view of predicting the chill cooling of steel droplets. A first model was developed by Rivaux [2011] whereas the present discusses a new model. The experimental work considered various facilities and environments to set a droplet of molten alloy in levitation: EML (fig. 1.8) for ground-based experiments, microgravity in parabolic flight or sounding rockets and last, microgravity condition on-board the International Space Station (ISS)



Fig. 1.8 – Electromagnetic levitation

1.4.2 Objectives and outline

The main focus of the present thesis is predicting macrosegregation with liquid dynamics assuming a fixed solid phase, i.e. no account of solid transport (e.g. equiaxed crystals sedimentation) and no account of solid deformation. In CEMEF, this scope has been adopted for previous work by Gouttebroze [2005], Liu [2005], Mosbah [2008], Rivaux [2011], and Carozzani [2012]. Nevertheless, many modelling features evolved with time such as going from two-dimensional to three-dimensional modelling, resolution schemes for each of the conservation equations: energy, chemical species and liquid momentum, Eulerian or Lagrangian descriptions, modelling of grain structure and others. In this thesis, we propose a numerical model that takes into account i) the energy conservation in a temperature formulation based on a thermodynamic database mapping, ii) the liquid momentum conservation with thermosolutal convection and solidification shrinkage as driving forces, iii) solute mass conservation and iv) solidification paths at full equilibrium for multicomponent alloys microsegregation. Moreover, all equations are formulated in a pure Eulerian description while using the Level Set method to keep implicitly track of the interface between the alloy and surrounding gas. To the author's knowledge, this work combining macrosegregation prediction using the level set methodology to track the metal-air interface during shrinkage has no precedent in casting and solidification literature.

Chapter 1. General Introduction

Numerical tools: Cimlib relying on PETSc, parallelized with MPICH2, paraview and python as tools for postprocess and analysis.

The previously mentionned simulation requirements are not met in a single casting software package. Nevertheless, *Thercast*® is a promising tool that already handles a part of the above points. The current thesis developments are done using C++ language as a part of the in-house code, known as *CimLib* [Digonnet et al. 2007; Mesri et al. 2009]. This fully parallel library is the main academic research support for *Thercast*®

Outline: each chapter content ...

Chapter 2

Modelling Review

Contents

2.1 Modelling macrosegregation	12
2.1.1 Dendritic growth	12
2.1.2 Mush permeability	12
2.1.3 Microsegregation	13
2.1.4 Macroscopic solidification model: monodomain	16
2.2 Eulerian and Lagrangian motion description	20
2.2.1 Overview	20
2.2.2 Interface capturing	21
2.3 Solidification models with level set	22
2.4 The level set method	22
2.4.1 Diffuse interface	23
2.4.2 Mixing Laws	24
2.4.3 Transport and regularisation	26
2.4.4 Interface Remeshing	28

2.1 Modelling macrosegregation

2.1.1 Dendritic growth

In a casting process, the chill surface i.e. the contact between the molten alloy and relatively cold moulds, is the first area to solidify. Thermal gradient, G , and cooling rate R are two crucial process parameters that define the interface speed \vec{v}^* , which in turn, affects the initial microstructure. Although it may be not easy to control them, it remains important to understand their implication in solidification.

The solid-liquid interface fluctuates when solidifying, thus perturbations may appear on the front, locally destabilizing it. Two outcome scenarios are possible. The first scenario is characterized by low values of \vec{v}^* where the interface maintains a planar shape, hence we speak of *planar growth*. With this kind of growth, a random protuberance appearing at the interface, has a low tip velocity (low driving force of solidification). As such, the rest of the interface catches up, keeping the planar geometry. In another scenario, where a real casting is considered, the interface speed is greater in general, due to high solidification rate. The protuberance tip will be pulled into a liquid less rich in solute than the interface. The zone ahead of the solid-liquid interface is constitutionally undercooled [Tiller et al. 1953], giving a greater driving force for the protuberance to grow in the direction of the thermal gradient. As it has a tree-like shape, we speak of *dendritic growth*. Near the chill surface, dendrites are columnar, with a favourable growth in the $<100>$ direction for alloys with cubic lattices, but different orientations are also reported in the literature [see Dantzig et al. 2009, p. 289]. If temperature is uniform, which is the case usually far from mould walls, a similar dendritic growth phenomenon occurs, but with an equiaxed morphology.

Columnar dendrites are characterized by a primary spacing, λ_1 , between the main trunks, and a secondary spacing, λ_2 , for the arms that are perpendicular to the trunks. It should be noted that λ_2 , together with the grain size, are two important microstructural parameters in the as-cast microstructure [Easton et al. 2011]. Further branching may occur but will not be discussed here.

2.1.2 Mush permeability

The dendritic geometry is crucial in solidification theory as it exhibits lower solid fraction compared to a microstructure formed by planar growth. This fact has consequences on the fluid-structure interaction in the mushy zone, namely the liquid flow through dendrites. At the chill surface, the solid grows gradually from dispersed growing nuclei to a permeable solid skeleton, until finally grains have fully grown at the end of phase change. The intermediate state where liquid can flow in and out of the mushy zone through the dendrites is a key phenomenon from a rheological perspective. The flow through the solid skeleton is damped by primary and secondary dendrites, resulting in momentum dissipation just like in saturated porous media. The famous Darcy [1856] law relates the pressure gradient ($\vec{\nabla}p$) to the fluid

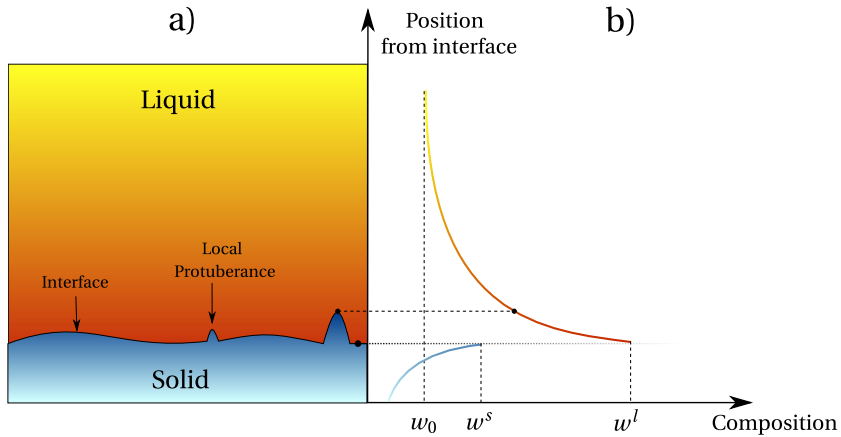


Fig. 2.1 – Schematic of a) a protuberance growing on the solid-liquid interface with b) the corresponding composition profiles (Reproduced and adapted from DoITPoMS [2000], © DoITPoMS, University of Cambridge).

velocity \vec{v} , through the following equation [Rappaz et al. 2003]:

$$\vec{v} = \frac{\mathbb{K}}{\mu^l} \vec{\nabla} p \quad (2.1)$$

where μ^l is the liquid dynamic viscosity and \mathbb{K} is the permeability tensor. The latter parameter has been the subject of numerous studies that aimed to predict it from various microstructural or morphological parameters. Some of these studies have started even before the first attempts to model macrosegregation by Flemings et al. [1967], Flemings et al. [1968a], and Flemings et al. [1968b]. Basically, all models include the solid fraction, g^s , as input to predict mush permeability along with empirical data. An instance of such models is the work of Xu et al. [1991]. Some models rely additionally on the primary dendrite arm spacing λ_1 like Blake-Kozeny [Ramirez et al. 2003], or the secondary dendrite arm spacing λ_2 like Carman-Kozeny, as a meaningful parameter to determine an isotropic permeability. Other models like Poirier [1987] and Felicelli et al. [1991] derive an anisotropic permeability based on both λ_1 and λ_2 . The present work uses Carman-Kozeny as a constitutive model for the isotropic permeability scalar (zero order tensor):

$$\mathbb{K} = \frac{\lambda_2^2 g^{l^3}}{180(1-g^l)^2} \quad (2.2)$$

2.1.3 Microsegregation

Microsegregation is a fundamental phenomenon in solidification. The simplest definition is an uneven distribution of solute between the liquid and the herein growing solid, at the microscopic scale of the interface separating these phases. If we consider a binary alloy, then the solubility limit is the key factor that dictates the composition at which a primary solid phase exists in equilibrium. The segregation (or partition) coefficient k determines the extent

of solute rejection into the liquid during solidification:

$$k = \frac{w^{s^*}}{w^{l^*}} \quad (2.3)$$

where w^{s^*} and w^{l^*} are the compositions of the solid and liquid respectively, at the interface. When the segregation coefficient is less than unity (such is the case for most alloys during dendritic solidification), the first solid forms with a composition $w^{s^*} = k w^{l^*} = k w_0$ less than the liquid's composition w_0 , the latter being initially at the nominal composition, w_0 . [Figure 2.2](#) illustrates a typical binary phase diagram where the real solidus and liquidus are represented by solid lines, while the corresponding linear approximations are in grey dashed lines. For most binary alloys, this linearisation simplifies derivation of microsegregation models, as k becomes independent of temperature.

For each phase, the relationship between the composition at the interface and that in the bulk depends on the chemical homogenisation ability of the phase. The more homogeneous a phase, the closer the concentrations between the interface and the bulk, hence closer to equilibrium. It is thus essential to study the effect of homogenisation on the segregation behaviour and the subsequent effect on solidification, which leads the formalism of microsegregation models.

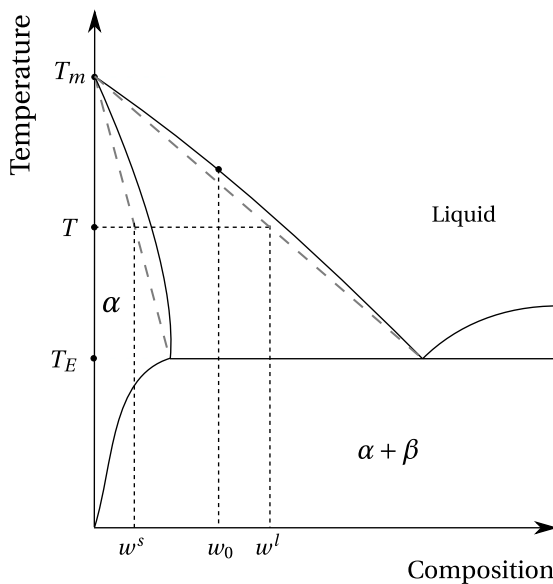


Fig. 2.2 – Typical eutectic phase diagram of a binary alloy showing the real solidus and liquidus at full equilibrium, with the corresponding linear approximations (grey dashed lines). T_m and T_E are respectively the melting point of the solvent and the eutectic temperature.

Microsegregation models

Solid formation depends greatly on the ability of chemicals species to diffuse within each of the solid and liquid phases, but also across the solid-liquid interface. Furthermore, chemical

diffusion like all other diffusional process, is a time-dependent phenomenon. One can thus conclude that two factors influence the amount of solid formation: cooling rate and diffusion coefficients. However, convection and other mechanical mixing sources, homogenise the composition much faster than atomic diffusion. As such, *complete mixing* in the liquid is always an acceptable assumption, regardless of the solidification time. We may speak of infinite diffusion in the liquid. Nevertheless, diffusion in the solid, also known as *back diffusion*, is the only transport mechanism with very low diffusion coefficients. Therefore, chemical species require a long time, i.e. low cooling rate, to completely diffuse within the solid. The difference in diffusional behaviour at the scale of a secondary dendrite arms, is summarized by two limiting segregation models of perfect equilibrium and nonequilibrium, which are the lever rule and Gulliver-Scheil models, respectively. Afterwards, models with finite back diffusion are presented.

in the three following sections, maybe I should add a small schematic next to each each equation to visualize concentration profiles

Lever rule

The lever rule considers an ideal equilibrium in all phases, i.e. solidification is extremely slow, hence phase compositions are homogeneous ($w^{l^*} = w^l$ and $w^{s^*} = w^s$) at all times as a consequence of complete mixing. These compositions are given by:

$$w^l = w^{l^*} = kw^{s^*} = kw^s \quad (2.4)$$

$$w^s = w^{s^*} = \frac{w_0}{k(1-f^s) + f^s} \quad (2.5)$$

At the end of solidification, the composition of the solid phase is equal to the nominal composition, $w^s = w_0$

Gulliver-Scheil

The other limiting case is the absence of diffusion in the solid. That includes also the diffusion at the interface, so nothing diffuses in or out. The consequence is a steady increase of the homogeneous liquid composition while the solid composition remains non-uniform. Compared to a full equilibrium approach, higher fractions of liquid will remain until eutectic composition is reached, triggering a eutectic solidification. The phase compositions are given by:

$$w^l = w^{l^*} = kw^{s^*} \quad (2.6)$$

$$w^s = kw_0(1-f^s)^{1-k} \quad (2.7)$$

Finite back diffusion

It has been concluded that the assumption of a negligible back diffusion overestimates the liquid composition and the resulting eutectic fraction. Therefore, many models studied the

limited diffusion in the solid. One of the earliest models is the Brody-Flemings models [Khan et al. 2014] that is based on a differential solute balance equation for a parabolic growth rate, as follows:

$$w^l = w^{l*} = kw^{s*} \quad (2.8)$$

$$w^s = kw_0 \left[1 - \left(1 - 2\text{Fo}^s k \right) f^s \right]^{\frac{k-1}{1-2\text{Fo}^s k}} \quad (2.9)$$

where Fo^s is the dimensionless *Fourier number* for diffusion in the solid [Dantzig et al. 2009]. It depends on the solid diffusion coefficient D^s , solidification time t_s and the secondary dendrite arm spacing, as follows:

$$\text{Fo}^s = \frac{D^s t_s}{(\lambda_2/2)^2} \quad (2.10)$$

Several other models were since suggested and used. The interested reader is referred to the following non exhaustive list of publications: Clyne et al. [1981], Kobayashi [1988], Ni et al. [1991], Wang et al. [1993], Combeau et al. [1996], Martorano et al. [2003], and Tourret et al. [2009]. It is noted that some of these publications consider also a finite diffusion in the liquid phase.

2.1.4 Macroscopic solidification model: monodomain

In this section, we will present the macroscopic conservations equations that enable us to predict macrosegregation in the metal when the latter is the only domain in the system.

Volume averaging

It is crucial for a solidification model to represent phenomena on the microscale, then scale up to predict macrscopic phenomena. Nevertheless, the characteristic length of a small scale in solidification may represent a dendrite arm spacing, for instance the mushy zone permeability, as it may also represent an atomic distance if one is interested, for instance, in the growth competition between diffusion and surface energy of the solid-liquid interface. Modelling infinitely small-scale phenomena could be prohibitively expensive in computation time, if we target industrial scales.

The volume averaging is a technique that allows bypassing this barrier by averaging small-scale variations on a so-called *representative volume element* (RVE) [Dantzig et al. 2009] of volume V_E , with the following dimensional constraints: the element should be large enough to "see" and average microscopic fluctuations whilst being smaller than the scale of macroscopic variations. Solid and liquid may exist simultaneously in the RVE, but no gas phase is considered (volume saturation: $V^s + V^l = V_E$). Moreover, temperature is assumed uniform and equal for all the phases. The formalism, introduced by Ni et al. [1991], is summarized by

the following equations for any physical quantity ψ :

$$\langle \psi \rangle = \frac{1}{V_E} \int_{V_E} \psi d\Omega = \langle \psi^s \rangle + \langle \psi^l \rangle \quad (2.11)$$

where $\langle \psi \rangle^s$ and $\langle \psi \rangle^l$ are phase averages of ψ . Then, for any phase ϕ , one can introduce the *phase intrinsic average* of ψ , denoted $\langle \psi \rangle^\phi$, by writing:

$$\langle \psi^\phi \rangle = \frac{1}{V_E} \int_{V^\phi} \psi d\Omega = g^\phi \langle \psi \rangle^\phi \quad (2.12)$$

where g^ϕ is the volume fraction of the phase. To finalize, the averaging is applied to temporal and spatial derivation operators [Rivaux 2011]:

$$\langle \frac{\partial \psi^\phi}{\partial t} \rangle = \frac{\partial \langle \psi^\phi \rangle}{\partial t} - \int_{\Gamma^*} \psi^\phi \vec{v}^* \cdot \vec{n}^\phi d\Gamma \quad (2.13)$$

$$\langle \vec{\nabla} \psi^\phi \rangle = \vec{\nabla} \langle \psi^\phi \rangle + \int_{\Gamma^*} \psi^\phi \vec{n}^\phi d\Gamma \quad (2.14)$$

where \vec{v}^* is the local relative interface velocity and Γ^* is the solid-liquid interface, while \vec{n}^ϕ is the normal to Γ^* , directed outwards. The surface integral term in eqs. (2.13) and (2.14) is an *interfacial average* that expresses exchanges between the phases across the interface. The previous equations will be used to derive a set macroscopic conservation equations. It is noted that the intrinsic average $\langle \psi \rangle^\phi$ may be replaced by ψ^ϕ for notation simplicity, whenever the averaging technique applies.

Macroscopic equations

A monodomain macroscopic model relies on four main conservation equations to predict macrosegregation in a single alloy domain, i.e. the latter is considered without any interaction with another alloy or ambient air. The general form of a conservation equation of any physical quantity ψ is given by [Rappaz et al. 2003]:

$$\frac{\partial \psi}{\partial t} + \nabla \cdot (\psi \vec{v}) - \nabla \cdot \vec{j}_\psi = Q_\psi \quad (2.15)$$

The first LHS term in eq. (2.15) represents the time variation of ψ , the second term accounts for transport by advection while the third is the diffusive transport and the RHS term represents a volume source. The considered equations are mass, energy, liquid momentum and species conservation, all summarized in table 2.1. The solid momentum is not considered as we assume a fixed and rigid solid phase ($\vec{v}^s = \vec{0}$). We develop the ingredients of these equations

Table 2.1 – Summary of conservation equations with their variables.

Conservation Equation	ψ	\vec{j}_ψ	Q_ψ
Mass	$\langle \rho \rangle$	–	–
Energy	$\langle \rho h \rangle$	$\langle \vec{q} \rangle$	–
Species	$\langle \rho w_i \rangle$	$\langle \vec{j}_i \rangle$	–
Liquid momentum	$\langle \rho \vec{v}^l \rangle$	$-\overline{\overline{\sigma^l}} \rangle$	\vec{F}_v^l

using the averaging technique, as follows:

$$\langle \rho \rangle = g^l \rho^l + g^s \rho^s \quad (2.16)$$

$$\langle \rho \vec{v} \rangle = g^l \rho^l \vec{v}^l + g^s \rho^s \vec{v}^s \quad (2.17)$$

$$\langle \rho h \rangle = g^l \rho^l h^l + g^s \rho^s h^s \quad (2.18)$$

$$\langle \rho h \vec{v} \rangle = g^l \rho^l h^l \vec{v}^l + g^s \rho^s h^s \vec{v}^s \quad (2.19)$$

$$\langle \rho w_i \rangle = g^l \rho^l w_i^l + g^s \rho^s w_i^s \quad (2.20)$$

$$\langle \rho w_i \vec{v} \rangle = g^l \rho^l w_i^l \vec{v}^l + g^s \rho^s w_i^s \vec{v}^s \quad (2.21)$$

Next, we define the average diffusive fluxes, \vec{q} for energy and \vec{j}_i for solutes, using Fourier's conduction law and Fick's first law, respectively:

$$\langle \vec{q} \rangle = -g^l \langle \kappa^l \rangle \vec{\nabla} T - g^s \langle \kappa^s \rangle \vec{\nabla} T \quad (2.22)$$

$$\langle \vec{j}_i \rangle = -g^l D^l \vec{\nabla} w_i^l - g^s D^s \vec{\nabla} w_i^s \quad (2.23)$$

In eq. (2.23), the solid diffusion coefficient is neglected, by considering that for macroscopic scales, the average composition of the alloy is much more influenced by advective and diffusive transport in the liquid. In eq. (2.22), we assumed that phases are at thermal equilibrium, that is, temperature is uniform in the RVE.

Now that the main conservation equations ingredients are properly defined, we may write each averaged conservation equations as the sum of two local conservation equations for each phase in the RVE, hence introducing also interfacial average terms. For instance, the local mass balance in each phase is given by:

$$\frac{\partial}{\partial t} \left(g^l \rho^l \right) + \nabla \cdot \left(g^l \rho^l \vec{v}^l \right) = S_V \langle \rho^l \vec{v}^{l*} \cdot \vec{n} \rangle^* - S_V \langle \rho^l \vec{v}^* \cdot \vec{n} \rangle^* \quad (2.24a)$$

$$\frac{\partial}{\partial t} \left(g^s \rho^s \right) + \nabla \cdot \left(g^s \rho^s \vec{v}^s \right) = -S_V \langle \rho^s \vec{v}^{s*} \cdot \vec{n} \rangle^* + S_V \langle \rho^s \vec{v}^* \cdot \vec{n} \rangle^* \quad (2.24b)$$

where $S_V = A_{sl}/V_E$ is the specific surface area, \vec{v}^{l*} and \vec{v}^{s*} are respectively, the liquid and solid phase velocity at the interface and \vec{v}^* is the previously introduced solid-liquid interface velocity. For instance, the first interfacial exchange term in the RHS of eq. (2.24a) is expanded as follows [Dantzig et al. 2009]:

I should adopt only one symbol for the differential inside the surface integrals dA or $d\Gamma$

$$S_V \langle \rho^l \vec{v}^{l*} \cdot \vec{n} \rangle^* = \frac{A_{sl}}{V_E} \left(\frac{1}{A_{sl}} \int_{A_{sl}} \rho^l \vec{v}^{l*} \cdot \vec{n} dA \right) \quad (2.25a)$$

$$= \frac{1}{V_E} \int_{A_{sl}} \rho^l \vec{v}^{l*} \cdot \vec{n} dA \quad (2.25b)$$

Summing equations (2.24a) and (2.24b), results in the overall mass balance in the RVE:

$$\frac{\partial}{\partial t} (g^l \rho^l + g^s \rho^s) + \nabla \cdot (g^l \rho^l \vec{v}^l + g^s \rho^s \vec{v}^s) = S_V \langle \rho^l (\vec{v}^{l*} - \vec{v}^*) \cdot \vec{n} \rangle^* - S_V \langle \rho^s (\vec{v}^{s*} - \vec{v}^*) \cdot \vec{n} \rangle^* \quad (2.26)$$

where the RHS cancels to zero as shown by Ni et al. [1991]. Moreover, the authors show that with their averaging technique, interfacial exchanges for energy, chemical species and momentum cancel out as they are equal in absolute value but opposite in sign. Using eqs. (2.16) to (2.23) and following the same procedure done in eq. (2.26), the averaged mass balance hence writes:

$$\frac{\partial \langle \rho \rangle}{\partial t} + \nabla \cdot \langle \rho \vec{v} \rangle = 0 \quad (2.27)$$

whereas the averaged energy balance writes:

$$\frac{\partial \langle \rho h \rangle}{\partial t} + \nabla \cdot \langle \rho h \vec{v} \rangle + \nabla \cdot (\langle \kappa \rangle \vec{\nabla} T) = 0 \quad (2.28)$$

and finally the species balance writes:

$$\frac{\partial \langle \rho w_i \rangle}{\partial t} + \nabla \cdot \langle \rho w_i \vec{v} \rangle + \nabla \cdot (g^l D^l \vec{\nabla} w_i^l) = 0 \quad (2.29)$$

As stated previously, the momentum balance in the solid phase is not taken into consideration, hence we do not sum the corresponding local conservation equations. The liquid momentum balance writes:

$$\frac{\partial}{\partial t} (\rho^l g^l \vec{v}^l) + \vec{\nabla} \cdot (\rho^l g^l \vec{v}^l \times \vec{v}^l) = \vec{\nabla} \cdot \left(g^l \overline{\sigma^l} \right) + g^l \vec{F}_v^l + \vec{\Gamma}^l \quad (2.30)$$

The interfacial momentum transfer between the solid and liquid phases is modelled by a momentum flux vector $\vec{\Gamma}^l$, consisting of hydrostatic and deviatoric parts, such that:

$$\vec{\Gamma}^l = \vec{\Gamma}_p^l + \vec{\Gamma}_{\mathbb{S}}^l \quad (2.31)$$

$$\vec{\Gamma}_p^l = p^{l*} \vec{\nabla} g^l = p^l \vec{\nabla} g^l \quad (2.32)$$

$$\vec{\Gamma}_{\mathbb{S}}^l = -g^{l2} \mu^l \mathbb{K}^{-1} (\vec{v}^l - \vec{\nu}^s) \quad (2.33)$$

where p^{l*} is the pressure at the interface, considered to be equal to the liquid hydrostatic pressure p^l , \mathbb{K} is a permeability scalar (isotropic) computed using eq. (2.1) and μ^l is the

liquid's dynamic viscosity. The general form of the Cauchy liquid stress tensor in [eq. \(2.30\)](#) is decomposed as follows:

$$\overline{\overline{\sigma^l}} = g^l \overline{\overline{\sigma^l}} = -\left(\langle p^l \rangle - \lambda \nabla \cdot \langle \vec{v}^l \rangle\right) \bar{\mathbb{I}} + \overline{\overline{\mathbb{S}}}^l \quad (2.34)$$

where λ is a dilatational viscosity [[Dantzig et al. 2009](#)] and $\overline{\overline{\mathbb{S}}}^l$ is the liquid strain deviator tensor. In the literature, the coefficient λ is taken proportional to the viscosity: $\lambda = \frac{2}{3}\mu^l$. However, as we consider an incompressible flow, the divergence term vanishes, thus rewriting [eq. \(2.34\)](#) as follows:

$$\overline{\overline{\sigma^l}} = -\langle p^l \rangle \bar{\mathbb{I}} + \overline{\overline{\mathbb{S}}}^l \quad (2.35a)$$

$$\overline{\overline{\sigma^l}} = -\langle p^l \rangle \bar{\mathbb{I}} + 2\mu^l \langle \dot{\epsilon}^l \rangle \quad (2.35b)$$

where the transition from [eq. \(2.35a\)](#) to [eq. \(2.35b\)](#) is made possible by assuming a Newtonian behaviour for the liquid phase. The strain rate tensor, $\langle \dot{\epsilon}^l \rangle$, depends on the average liquid velocity:

$$\langle \dot{\epsilon}^l \rangle = \frac{1}{2} \left(\overline{\overline{\nabla}} \langle \vec{v}^l \rangle + \overline{\overline{\nabla^t}} \langle \vec{v}^l \rangle \right) \quad (2.36)$$

Macro models: Rivaux ? Gu beckermann 1999

Micro macro: Tommy Carozzani 2013, guo beckermann 2003, Combeau 2009, Miha Zaloznik 2010 (indirect), P. Thévoz, J.-L. Desbiolles, M. Rappaz, Metallurgical and Materials Transactions A 20 (2) (1989) 311–322

end by talking about taking air into account and the need for an interface capturing method

2.2 Eulerian and Lagrangian motion description

2.2.1 Overview

In mechanics, it is possible to describe motion using two well-known motion description: Eulerian and Lagrangian descriptions. To start with the latter, it describes the motion of a particle by attributing a reference frame that moves with the particle. In other words, the particle itself is the center of a reference frame moving at the same speed during time. The position, denoted x , is hence updated as follows:

$$x^{(t+1)} = x^{(t)} + \vec{v} \Delta t \quad (2.37)$$

As such, the total variation of any physical quantity ψ related to the particle can be found by deriving with respect to time, $\frac{d\psi}{dt}$. In contrast to the Lagrangian description, the Eulerian description considers a fixed reference frame and independent of the particle's trajectory. The total variation of ψ cannot be simply described by a temporal derivative, since the particle's velocity is not known to the reference frame, and thus the velocity effect, namely the advective

transport of ψ , should also be considered as follows:

$$\frac{d\psi}{dt} = \frac{\partial\psi}{\partial t} + \underbrace{\vec{v} \cdot \vec{\nabla}\psi}_{\text{Advection Transport}} \quad (2.38)$$

In this case, the LHS term is also known as *total* or *material derivative*.

The importance of these motion descriptions is essential to solve mechanics, whether for fluids or solids, using a numerical method like the finite element method (FEM). One of the main steps of this method is to spatially discretise a continuum into a grid of points (nodes, vertices ...), where any physical field shall be accordingly discretized. Now, if we focus on a node where velocity has a non zero value and following the previously made analysis, two outcomes are possible: either the node would be fixed (Eulerian) or it would move by a distance proportional to the prescribed velocity (Lagrangian). In the latter case, points located on the boundaries constantly require an update of the imposed boundary conditions.

From these explanations, one can deduce that an Eulerian framework is suited for fluid mechanics problems where velocities are high and may distort the mesh points, whereas the Lagrangian framework is better suited for solid mechanics problems where deformation velocities are relatively low and should well behave when predicting strains.

Another motion description has emerged some decades ago, [Hirt \[1971\]](#) call it the Arbitrary Langrangian-Eulerian (ALE) method. ALE combines advantages from both previous descriptions as it dictates a Lagrangian behavior at "solid" nodes where solid is deforming, and an Eulerian behavior at "fluid" nodes.

2.2.2 Interface capturing

As no solid deformation is considered in this work, the Eulerian framework is a convenient choice. Although solidification shrinkage is to be considered in the current scope, it will deform the alloy's outer surface in contact with the air. We intend to track this interface and its motion over time via a numerical method. A wide variety of methods accomplish this task while they yield different advantages and disadvantages. Such methods fall into two main classes, either interface tracking or interface capturing, among which we cite: marker-and-cell (MAC) [[Harlow et al. 1965](#)], volume of fluid (VOF) [[Hirt et al. 1981](#)], phase field methods (PF), level set method (LSM) [[Osher et al. 1988](#)], coupled level set - VOF method and others. The interested reader may refer to quick references by [Prosperetti \[2002\]](#) and [Maitre \[2006\]](#) about these methods.

In the past years, the level set method received a considerable attention in many computational fields, specifically in solidification. For this reason, we will focus on this method henceforth, giving a brief literature review and technical details in the next sections.

2.3 Solidification models with level set

In classic solidification problems, the need to track an interface occurs usually at the solid-liquid interface, that is why the phase field method [Karma et al. 1996; Boettinger et al. 2002] and the level set method [Chen et al. 1997; Gibou et al. 2003; Tan et al. 2007] were applied at a microscale to follow mainly the dendritic growth of a single crystal in an undercooled melt. In our case however, when we mention "solidification models using LSM", we do not mean the solid-liquid interface inside the alloy, but it is the alloy(liquid)-air interface that is tracked, assuming that microscale phenomena between the phases within the alloy, are averaged using the previously defined technique in section 2.1.4.

Very few models were found in the literature, combining solidification and level set as stated previously. Du et al. [2001] applied it to track the interface between two molten alloys in a double casting technique. Welding research, on another hand, has been more active adapting the level set methodology to corresponding applications. In CEMEF, two projects use the metal-air level set methodology in welding simulations and showed promising results.

two sentences not more about the contribution of OD and SC

Firstly, Desmaison et al. [2014] ... TODO

Later, Chen [2014] applied it to gas metal arc welding (GMAW) to predict the grain structure in the heat affected zone essentially. More recently, Courtois et al. [2014] used the same methodology but this time to predict keyhole defect formation in spot laser welding. The tracked interface in this case was that between the molten alloy and the corresponding vapor phase.

2.4 The level set method

Firstly introduced by Osher et al. [1988], this method became very popular in studying multiphase flows. It is reminded that the term *multiphase* in computational domains usually refers to multiple fluids, and thus should not be mixed with definition of a phase in the current solidification context. For disambiguation, we shall use *multifluid flow* when needed. The great advantage lies in the way the interface between two fluids, F_1 and F_2 is implicitly captured, unlike other methods where the exact interface position is needed. In a discrete domain, the concept is to assign for each mesh node of position x , the minimum distance $d_\Gamma(x)$ separating it from an interface Γ . The distance function, denoted α and defined in eq. (2.39), is then signed positive or negative, based on the fluid or domain to which the node belongs.

$$\alpha(x) = \begin{cases} d_\Gamma(x) & \text{if } x \in F_1 \\ -d_\Gamma(x) & \text{if } x \in F_2 \\ 0 & \text{if } x \in \Gamma_{F1,F2} \end{cases} \quad (2.39)$$

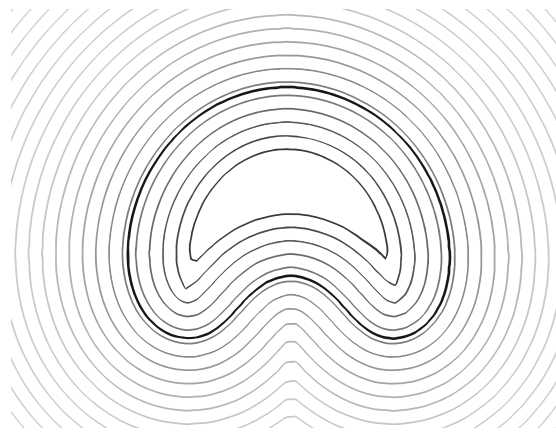


Fig. 2.3 – Schematic of the interface (thick black line) of a rising air bubble in water. The other contours represent isovalues of the distance function around and inside the interface contour.

2.4.1 Diffuse interface

The level set has many attractive properties that allows seamless implementation in 2D and 3D models. It is a continuously differentiable C^1 -function. For instance, a *Heaviside* function, denoted H , can be obtained by first order derivation of the level set function. The Heaviside function is continuous but non differentiable, with an abrupt transition from 0 to 1 across the sharp interface, as follows:

$$H = \begin{cases} 0 & \text{if } \alpha(x) < 0 \\ 1 & \text{if } \alpha(x) \geq 0 \end{cases} \quad (2.40)$$

With the help of eq. (2.40), we can define the geometric "presence" of a domain with respect to the interface. As such, material properties depend upon this function, which will be discussed later in section 2.4.2. It is established that a steep transition can lead to numerical problems, so the Heaviside function should be smoothed in a fixed thickness. Sinusoidal smoothing in eq. (2.41) is widely used with level set formulations.

$$H = \begin{cases} 0 & \text{if } \alpha(x) < -\epsilon \\ 1 & \text{if } \alpha(x) > \epsilon \\ \frac{1}{2} \left(1 + \frac{\alpha(x)}{\epsilon} + \frac{1}{\epsilon} \sin \left(\frac{\pi \alpha(x)}{\epsilon} \right) \right) & \text{if } -\epsilon \leq \alpha(x) \leq \epsilon \end{cases} \quad (2.41)$$

where the interval $[-\epsilon; \epsilon]$ is an artificial interface thickness around the zero distance. Defining a diffuse interface rather than a sharp one, is also a common approach in phase field methods [Beckermann et al. 1999; Sun et al. 2004]. It is emphasized that the latter methods give physically meaningful analysis of a diffuse interface and the optimal thickness by thoroughly studying the intricate phenomena happening at the scale of the interface. However, for level set methods, there has not been a formal work leading the same type of analysis. For this reason, many aspects of the level set method lack physical meanings but still computationally

useful. In a recent paper by Gada et al. [2009], the authors respond partially to this problem by analysing and deriving conservation equations using a level set in a more meaningful way, but do not discuss the diffuse interface aspect.

add two sentences about dirac and curvature, as properties that can be readily obtained from the level set

Finally, within the diffuse interface, fluids properties may vary linearly or not, depending on the mixing law, which is presented in the next section.

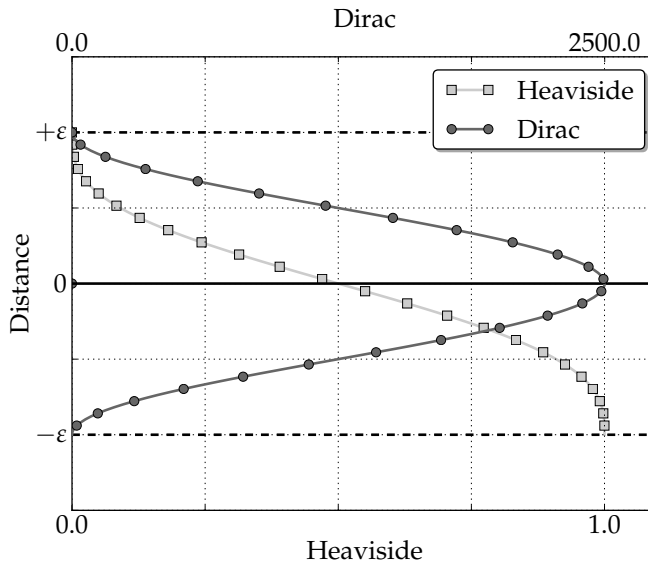


Fig. 2.4 – Schematic of two level properties inside the diffuse interface: Heaviside (lower x-axis) and Dirac delta (upper x-axis) functions. In this example, the interface thickness is 800 μm .

2.4.2 Mixing Laws

A *monolithic* resolution style, as opposed to a *partitioned* resolution, is based on solving a single set of equations for both fluids separated by an interface, as if a single fluid were considered. Level set is one many methods that use the monolithic style to derive a single set of conservation equations for both fluids. The switch from one material to the other is implicitly taken care of by using the Heaviside function as well mixing laws. These laws are crucial to define how properties vary across the diffuse interface in view of a more accurate resolution. The most frequently used mixing law in the literature is the arithmetic law. Other transitions are less known such as the harmonic and logarithmic mixing. The first law is maybe the most intuitive and most used for properties mixture as it emanates from VOF-based methods. If we consider any property ψ , for instance the fluid's dynamic viscosity μ , then the arithmetic law will give a mixed property $\hat{\psi}$ as follows:

$$\hat{\psi} = H^{F_1} \psi^{F_1} + H^{F_2} \psi^{F_2} \quad (2.42)$$

Basically, the result is an average property that follows the same trend as the Heaviside function. As for the harmonic law, it writes:

$$\widehat{\psi} = \left(\frac{H^{F_1}}{\psi^{F_1}} + \frac{H^{F_2}}{\psi^{F_2}} \right)^{-1} \quad (2.43)$$

and last, the logarithmic law writes:

$$\widehat{\psi} = n^{(H^{F_1} \log_n \psi^{F_1} + H^{F_2} \log_n \psi^{F_2})} \quad (2.44)$$

where n is any real number serving as a logarithm base, which often is either the exponential e or 10. The mixture result with this law is the same, regardless of the value of n . By looking to [fig. 2.5](#), we clearly see that the difference between all three approaches is the property weight given to each side of the level set in the mixture. The arithmetic law, being symmetric, has equal weights, ψ^{F_1} and ψ^{F_2} , in the final mixture. Nevertheless, the asymmetric harmonic mixing varies inside the diffuse interface with a dominant weight of one property over the other. As for the logarithmic mixture, it can be seen as an intermediate transition between the preceding laws. As long as the interface thickness is small enough, the choice of a mixing

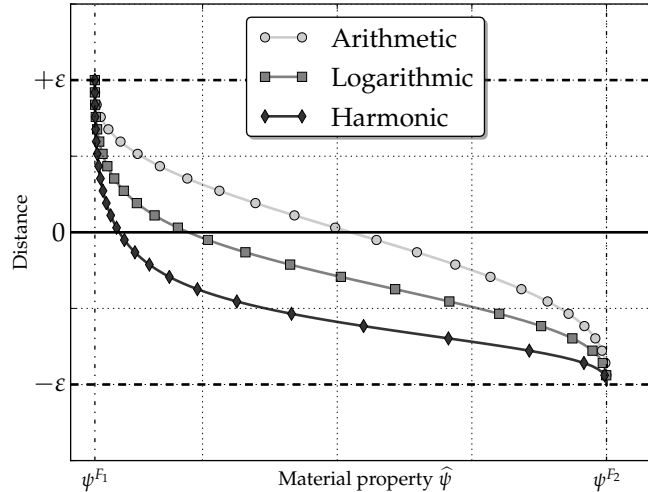


Fig. 2.5 – Three mixing laws, arithmetic, logarithmic and harmonic commonly used in monolithic formulations.

law should not drastically change the result, inasmuch as it depends on the discretisation resolution of the interface. This fact made the arithmetic mixing the most applied one, because it is symmetric and easy to implement (no handling of potential division problems like harmonic laws for instance). However, [Strotos et al. \[2008\]](#) claim that the harmonic law proves to conserve better diffusive fluxes at the interface. More recently, an interesting study made by [Ettrich et al. \[2014\]](#) focused on mixing thermal properties using a phase field method. They define a diffuse interface in which they separately mix the thermal conductivity, κ , and the heat capacity, C_v , then compute the thermal diffusivity as the ratio of these properties. Later, the authors compare the temperature field obtained by diffusion to a reference case in order

to decide which combination of mixing laws gives the best result. Despite not being directly related to a level set method, this work gives an insight of the mixture possibilities and their effect on a pure thermal diffusion. Otherwise, little work has been found in the literature on the broad effects of mixture types on simulation results in a level set context.

2.4.3 Transport and regularisation

When a physical interface needs to have topology changes because of fluid structure interaction or surface tension for instance, the level set model can easily follow these changes by a transport step. The idea is to advect the signed distance function, its zero isovalue representing the interface and all other distant isovales, with the velocity field as input. The problem can be simply written as:

$$\frac{d\alpha}{dt} = \frac{\partial\alpha}{\partial t} + \vec{v} \cdot \vec{\nabla}\alpha = 0 \quad (2.45)$$

Associated boundary conditions

Transport formulation

The finite element method gives the fully discretised weak form of eq. (2.45) by writing:

$$\int_{\Omega} \alpha^* \frac{\partial\alpha}{\partial t} d\Omega + \int_{\Omega} \alpha^* \vec{v} \cdot \vec{\nabla}\alpha d\Omega = 0 \quad \forall \alpha^* \in \mathcal{H}^1(\Omega) \quad (2.46)$$

If we opt for a forward finite difference for time discretisation and the following nodal discretisation in space, assuming N the number of nodes in any simplex:

$$\alpha = \sum_N N_j \alpha_j \quad (2.47)$$

then eq. (2.46) can be recast as follows:

continue weak form discretisation

$$\frac{1}{\Delta t} \alpha_j \int_{\Omega} N_i N_j d\Omega + \alpha_j \int_{\Omega} \vec{v} \cdot \vec{\nabla} N_j d\Omega = 0 \quad (2.48)$$

Regularisation

Upon transport the distance function field, a crucial property of the level set may be partially or totally lost over the domain, which is:

$$\|\vec{\nabla}\alpha\| = 1 \quad (2.49)$$

The closer this L^2 -norm to one, the more regular the level set. An irregular distance function cannot accurately capture the physical interface and thus results in numerical errors, because

of wrong distance information. When the transport equation in eq. (2.45) is discretised in time then solved, a *regularisation* (also known as *reinitialisation*) is necessary to conserve as much as possible the property in eq. (2.49).

Figure 2.6 shows the need of regularisation in two different simulations of the same phenomenon: rising air bubble inside water. The importance of this well studied case [Hysing et al. 2009] is that the interface between two fluids is highly deformable as the bubble rises because of buoyancy, and therefore the task of tracking the dynamic interface while maintaining an accurate distance function is a considerable numerical task. In the first simulation, the distance contours are squeezed against the zero-distance contour marked by the thick black line. A closer look to the interface reveals undesired distortions, with a "wavy" shape at some points. This effect is evidently an artefact of a level set transport lacking subsequent reinitialisation, inasmuch as the surface tension tends to minimise the total surface area and make it as smooth as possible. Nevertheless, the second simulation unveils much better results, especially how the interface shows no sign of destabilisation. We also note the regular spacing between contours, which is a consequence of conserving the property defined in eq. (2.49). We attribute this improvement to the regularization done at each time step after the transport. In the forthcoming sections, we present two regularisation methods, then show their strong and weak points.

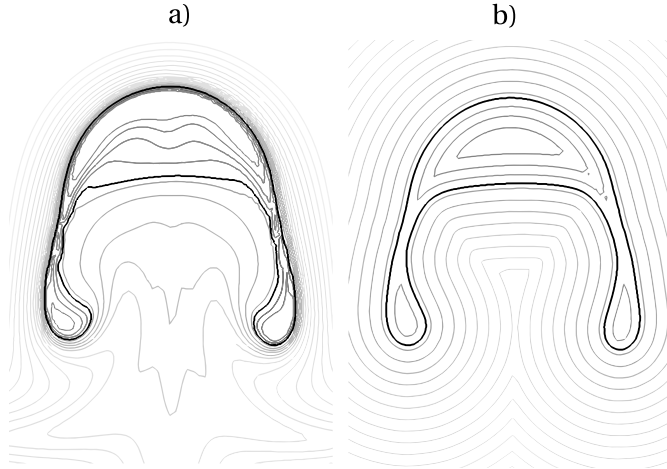


Fig. 2.6 – Schematic of the influence of level set regularisation on the distance function at the same time frame: a) without any regularisation step, the isovalue contours are distorted in the wake of the rising air bubble while being squeezed ahead of it, b) in contrast to regularising the distance function, where the contours maintain their spacing and geometric properties with respect to the tracked interface.

Numerical stability

Convective reinitialisation and Hamilton-Jacobi equations

Geometric reinitialization

2.4.4 Interface Remeshing

Importance when using a static level set and more importantly when LS is transported, influence of mixing area *thickness* and *resolution* (i.e. nb of nodes with the area), Isotropic or anisotropic ? the first is more important to composition calculation while the second is more relevant if we mean do thermohydraulics without macrosegregation

Bibliography

[Beckermann 2002]

Beckermann, C. (2002). "Modelling of macrosegregation: applications and future needs". *International Materials Reviews*, 47 (5), pp. 243–261. URL: <http://www.maneyonline.com/doi/abs/10.1179/095066002225006557> (cited on page 5).

[Beckermann et al. 1999]

Beckermann, C, H. J Diepers, I Steinbach, A Karma, and X Tong (1999). "Modeling Melt Convection in Phase-Field Simulations of Solidification". *Journal of Computational Physics*, 154 (2), pp. 468–496. URL: <http://www.sciencedirect.com/science/article/pii/S0021999199963234> (cited on page 23).

[Boettinger et al. 2002]

Boettinger, W. J., J. A. Warren, C. Beckermann, and A. Karma (2002). "Phase-Field Simulation of Solidification1". *Annual Review of Materials Research*, 32 (1), pp. 163–194. URL: <http://dx.doi.org/10.1146/annurev.matsci.32.101901.155803> (cited on page 22).

[Carozzani 2012]

Carozzani, T. (2012). "Développement d'un modèle 3D Automate Cellulaire-Éléments Finis (CAFE) parallèle pour la prédiction de structures de grains lors de la solidification d'alliages métalliques". PhD thesis. Ecole Nationale Supérieure des Mines de Paris. URL: <http://pastel.archives-ouvertes.fr/pastel-00803282> (cited on page 9).

[Chen et al. 1997]

Chen, S., B. Merriman, S. Osher, and P. Smereka (1997). "A Simple Level Set Method for Solving Stefan Problems". *Journal of Computational Physics*, 135 (1), pp. 8–29. URL: <http://www.sciencedirect.com/science/article/pii/S0021999197957211> (cited on page 22).

[Chen 2014]

Chen, S. (2014). "Three dimensional Cellular Automaton - Finite Element (CAFE) modeling for the grain structures development in Gas Tungsten / Metal Arc Welding processes". Theses. Ecole Nationale Supérieure des Mines de Paris. URL: <https://pastel.archives-ouvertes.fr/pastel-01038028> (cited on page 22).

[Clyne et al. 1981]

Clyne, T. W. and W. Kurz (1981). "Solute redistribution during solidification with rapid solid state diffusion". *Metallurgical Transactions A*, 12 (6), pp. 965–971. URL: <http://link.springer.com/article/10.1007/BF02643477> (cited on page 16).

Bibliography

[Combeau et al. 1996]

Combeau, H., J.-M. Drezet, A. Mo, and M. Rappaz (1996). “Modeling of microsegregation in macrosegregation computations”. *Metallurgical and Materials Transactions A*, 27 (8), pp. 2314–2327. URL: <http://link.springer.com/article/10.1007/BF02651886> (cited on page 16).

[Combeau et al. 2009]

Combeau, H., M. Založnik, S. Hans, and P. E. Richy (2009). “Prediction of Macrosegregation in Steel Ingots: Influence of the Motion and the Morphology of Equiaxed Grains”. *Metallurgical and Materials Transactions B*, 40 (3), pp. 289–304. URL: <http://link.springer.com/article/10.1007/s11663-008-9178-y> (cited on page 6).

[Courtois et al. 2014]

Courtois, M., M. Carin, P. L. Masson, S. Gaied, and M. Balabane (2014). “A complete model of keyhole and melt pool dynamics to analyze instabilities and collapse during laser welding”. *Journal of Laser Applications*, 26 (4), p. 042001. URL: <http://scitation.aip.org/content/jlia/journal/jla/26/4/10.2351/1.4886835> (cited on page 22).

[Dantzig et al. 2009]

Dantzig, J. A. and M. Rappaz (2009). *Solidification*. EPFL Press (cited on pages 2, 12, 16, 18, 20).

[Darcy 1856]

Darcy, H. (1856). *Les fontaines publiques de la ville de Dijon : exposition et application des principes à suivre et des formules à employer dans les questions de distribution d'eau*. V. Dalmont (Paris). URL: <http://gallica.bnf.fr/ark:/12148/bpt6k624312> (cited on page 12).

[Desmaison et al. 2014]

Desmaison, O., M. Bellet, and G. Guillemot (2014). “A level set approach for the simulation of the multipass hybrid laser/GMA welding process”. *Computational Materials Science*, 91, pp. 240–250. URL: <http://www.sciencedirect.com/science/article/pii/S092702561400278X> (cited on page 22).

[Digonnet et al. 2007]

Digonnet, H., L. Silva, and T. Coupez (2007). “Cimlib: A Fully Parallel Application For Numerical Simulations Based On Components Assembly”. *AIP Conference Proceedings*. Vol. 908. AIP Publishing, pp. 269–274. URL: <http://scitation.aip.org/content/aip/proceeding/aipcp/10.1063/1.2740823> (cited on page 10).

[DoITPoMS 2000]

DoITPoMS (2000). *Dissemination of IT for the Promotion of Materials Science*. URL: <http://www.doitpoms.ac.uk/> (cited on page 13).

[Du et al. 2001]

Du, Q., D. Li, Y. Li, R. Li, and P. Zhang (2001). “Simulating a double casting technique using level set method”. *Computational Materials Science*, 22 (3–4), pp. 200–212. URL: <http://www.sciencedirect.com/science/article/pii/S0927025601001902> (cited on page 22).

[Easton et al. 2011]

Easton, M., C. Davidson, and D. StJohn (2011). “Grain Morphology of As-Cast Wrought Aluminium Alloys”. *Materials Transactions*, 52 (5), pp. 842–847 (cited on page 12).

[Ettrich et al. 2014]

Ettrich, J. et al. (2014). "Modelling of transient heat conduction with diffuse interface methods". *Modelling and Simulation in Materials Science and Engineering*, 22 (8), p. 085006. URL: <http://iopscience.iop.org/0965-0393/22/8/085006> (cited on page 25).

[Felicelli et al. 1991]

Felicelli, S. D., J. C. Heinrich, and D. R. Poirier (1991). "Simulation of freckles during vertical solidification of binary alloys". *Metallurgical Transactions B*, 22 (6), pp. 847–859. URL: <http://link.springer.com/article/10.1007/BF02651162> (cited on pages 6, 13).

[Flemings 1974]

Flemings, M. C. (1974). "Solidification processing". *Metallurgical Transactions*, 5 (10), pp. 2121–2134. URL: <http://link.springer.com/article/10.1007/BF02643923> (cited on page 6).

[Flemings et al. 1967]

Flemings, M. C. and G. E. Nereo (1967). "Macrosegregation: Part I". *Transactions of the Metallurgical Society of AIME*, 239, pp. 1449–1461 (cited on page 13).

[Flemings et al. 1968a]

Flemings, M. C., R. Mehrabian, and G. E. Nereo (1968a). "Macrosegregation: Part II". *Transactions of the Metallurgical Society of AIME*, 242, pp. 41–49 (cited on page 13).

[Flemings et al. 1968b]

Flemings, M. C. and G. E. Nereo (1968b). "Macrosegregation: Part III". *Transactions of the Metallurgical Society of AIME*, 242, pp. 50–55 (cited on page 13).

[Gada et al. 2009]

Gada, V. H. and A. Sharma (2009). "On Derivation and Physical Interpretation of Level Set Method-Based Equations for Two-Phase Flow Simulations". *Numerical Heat Transfer, Part B: Fundamentals*, 56 (4), pp. 307–322. URL: <http://dx.doi.org/10.1080/10407790903388258> (cited on page 24).

[Giamei et al. 1970]

Giamei, A. F. and B. H. Kear (1970). "On the nature of freckles in nickel base superalloys". *Metallurgical Transactions*, 1 (8), pp. 2185–2192. URL: <http://link.springer.com/article/10.1007/BF02643434> (cited on page 6).

[Gibou et al. 2003]

Gibou, E., R. Fedkiw, R. Caflisch, and S. Osher (2003). "A Level Set Approach for the Numerical Simulation of Dendritic Growth". *Journal of Scientific Computing*, 19 (1-3), pp. 183–199. URL: <http://link.springer.com/article/10.1023/A%3A1025399807998> (cited on page 22).

[Gouttebroze 2005]

Gouttebroze, S. (2005). "Modélisation 3d par éléments finis de la macroségrégation lors de la solidification d'alliages binaires". PhD thesis. École Nationale Supérieure des Mines de Paris. URL: <https://pastel.archives-ouvertes.fr/pastel-00001885/document> (cited on page 9).

[Harlow et al. 1965]

Harlow, F. H. and J. E. Welch (1965). "Numerical Calculation of Time-Dependent Viscous Incom-

Bibliography

pressible Flow of Fluid with Free Surface". *Physics of Fluids* (1958-1988), 8 (12), pp. 2182–2189.
URL: <http://scitation.aip.org/content/aip/journal/pof1/8/12/10.1063/1.1761178> (cited on page 21).

[Hirt 1971]

Hirt, C. W. (1971). "An arbitrary Lagrangian-Eulerian computing technique". *Proceedings of the Second International Conference on Numerical Methods in Fluid Dynamics*. Ed. by M. Holt. Lecture Notes in Physics 8. Springer Berlin Heidelberg, pp. 350–355. URL: http://link.springer.com/chapter/10.1007/3-540-05407-3_50 (cited on page 21).

[Hirt et al. 1981]

Hirt, C. W and B. D Nichols (1981). "Volume of fluid (VOF) method for the dynamics of free boundaries". *Journal of Computational Physics*, 39 (1), pp. 201–225. URL: <http://www.sciencedirect.com/science/article/pii/0021999181901455> (cited on page 21).

[Hysing et al. 2009]

Hysing, S. et al. (2009). "Quantitative benchmark computations of two-dimensional bubble dynamics". *International Journal for Numerical Methods in Fluids*, 60 (11), pp. 1259–1288. URL: <http://onlinelibrary.wiley.com/doi/10.1002/fld.1934/abstract> (cited on page 27).

[Karma et al. 1996]

Karma, A. and W.-J. Rappel (1996). "Phase-field method for computationally efficient modeling of solidification with arbitrary interface kinetics". *Physical Review E*, 53 (4), R3017–R3020. URL: <http://link.aps.org/doi/10.1103/PhysRevE.53.R3017> (cited on page 22).

[Khan et al. 2014]

Khan, M. I., A. O. Mostafa, M. Aljarrah, E. Essadiqi, and M. Medraj (2014). "Influence of Cooling Rate on Microsegregation Behavior of Magnesium Alloys". *Journal of Materials*, 2014, e657647. URL: <http://www.hindawi.com/journals/jma/2014/657647/abs/> (cited on page 16).

[Kobayashi 1988]

Kobayashi, S. (1988). "Solute redistribution during solidification with diffusion in solid phase: A theoretical analysis". *Journal of Crystal Growth*, 88 (1), pp. 87–96. URL: <http://www.sciencedirect.com/science/article/pii/S0022024898900100> (cited on page 16).

[Kohler 2008]

Kohler, F. (2008). "Peritectic solidification of Cu-Sn alloys: microstructure competition at low speed". PhD thesis. EPFL (cited on page 4).

[Lesoult 2005]

Lesoult, G. (2005). "Macrosegregation in steel strands and ingots: Characterisation, formation and consequences". *Materials Science and Engineering: A*, International Conference on Advances in Solidification Processes 413–414, pp. 19–29. URL: <http://www.sciencedirect.com/science/article/pii/S0921509305010063> (cited on page 6).

[Liu 2005]

Liu, W. (2005). "Finite Element Modelling of Macrosegregation and Thermomechanical Phenomena in Solidification Processes". PhD thesis. École Nationale Supérieure des Mines de Paris. URL: <http://pastel.archives-ouvertes.fr/pastel-00001339> (cited on page 9).

[Maitre 2006]

Maitre, E. (2006). "Review of numerical methods for free interfaces". Les Houches, France. URL: <http://goo.gl/Re6f3a> (cited on page 21).

[Martorano et al. 2003]

Martorano, M. A., C. Beckermann, and C.-A. Gandin (2003). "A solutal interaction mechanism for the columnar-to-equiaxed transition in alloy solidification". *Metallurgical and Materials Transactions A*, 34 (8), pp. 1657–1674. URL: <http://link.springer.com/article/10.1007/s11661-003-0311-x> (cited on page 16).

[Mesri et al. 2009]

Mesri, Y., H. Digonnet, and T. Coupez (2009). "Advanced parallel computing in material forming with CIMLib". *European Journal of Computational Mechanics/Revue Européenne de Mécanique Numérique*, 18 (7-8), pp. 669–694. URL: <http://www.tandfonline.com/doi/abs/10.3166/ejcm.18.669-694> (cited on page 10).

[Mosbah 2008]

Mosbah, S. (2008). "Multiple scales modeling of solidification grain structures and segregation in metallic alloys". PhD thesis. École Nationale Supérieure des Mines de Paris. URL: <https://tel.archives-ouvertes.fr/tel-00349885/document> (cited on page 9).

[Ni et al. 1991]

Ni, J. and C. Beckermann (1991). "A volume-averaged two-phase model for transport phenomena during solidification". *Metallurgical Transactions B*, 22 (3), pp. 349–361. URL: <http://link.springer.com/article/10.1007/BF02651234> (cited on pages 16, 19).

[Osher et al. 1988]

Osher, S. and J. A. Sethian (1988). "Fronts propagating with curvature-dependent speed: Algorithms based on Hamilton-Jacobi formulations". *Journal of Computational Physics*, 79 (1), pp. 12–49. URL: <http://www.sciencedirect.com/science/article/pii/0021999188900022> (cited on pages 21, 22).

[Poirier 1987]

Poirier, D. R. (1987). "Permeability for flow of interdendritic liquid in columnar-dendritic alloys". *Metallurgical Transactions B*, 18 (1), pp. 245–255. URL: <http://link.springer.com/article/10.1007/BF02658450> (cited on page 13).

[Prosperetti 2002]

Prosperetti, A. (2002). "Navier-Stokes Numerical Algorithms for Free-Surface Flow Computations: An Overview". *Drop-Surface Interactions*. Ed. by M. Rein. CISM International Centre for Mechanical Sciences 456. Springer Vienna, pp. 237–257. URL: http://link.springer.com/chapter/10.1007/978-3-7091-2594-6_8 (cited on page 21).

[Ramirez et al. 2003]

Ramirez, J. C. and C. Beckermann (2003). "Evaluation of a rayleigh-number-based freckle criterion for Pb-Sn alloys and Ni-base superalloys". *Metallurgical and Materials Transactions A*, 34 (7), pp. 1525–1536. URL: <http://link.springer.com/article/10.1007/s11661-003-0264-0> (cited on page 13).

Bibliography

[Rappaz et al. 2003]

Rappaz, M., M. Bellet, and M. Deville (2003). *Numerical Modeling in Materials Science and Engineering*. Springer Series in Computational Mathematics. Springer Berlin Heidelberg (cited on pages 13, 17).

[Rivaux 2011]

Rivaux, B. (2011). "Simulation 3D éléments finis des macroségrégations en peau induites par déformations thermomécaniques lors de la solidification d'alliages métalliques". PhD thesis. École Nationale Supérieure des Mines de Paris. URL: <http://pastel.archives-ouvertes.fr/pastel-00637168> (cited on pages 9, 17).

[Sarazin et al. 1992]

Sarazin, J. R. and A. Hellawell (1992). "Studies of Channel-Plume Convection during Solidification". *Interactive Dynamics of Convection and Solidification*. Ed. by S. H. Davis, H. E. Huppert, U. Müller, and M. G. Worster. NATO ASI Series 219. Springer Netherlands, pp. 143–145. URL: http://link.springer.com/chapter/10.1007/978-94-011-2809-4_22 (cited on page 3).

[Schneider et al. 1997]

Schneider, M. C., J. P. Gu, C. Beckermann, W. J. Boettinger, and U. R. Kattner (1997). "Modeling of micro- and macrosegregation and freckle formation in single-crystal nickel-base superalloy directional solidification". *Metallurgical and Materials Transactions A*, 28 (7), pp. 1517–1531. URL: <http://link.springer.com/article/10.1007/s11661-997-0214-3> (cited on page 3).

[Shevchenko et al. 2013]

Shevchenko, N., S. Boden, G. Gerbeth, and S. Eckert (2013). "Chimney Formation in Solidifying Ga-25wt pct In Alloys Under the Influence of Thermosolutal Melt Convection". *Metallurgical and Materials Transactions A*, 44 (8), pp. 3797–3808. URL: <http://link.springer.com/article/10.1007/s11661-013-1711-1> (cited on page 3).

[Strotos et al. 2008]

Strotos, G., M. Gavaises, A. Theodorakatos, and G. Bergeles (2008). "Numerical investigation of the cooling effectiveness of a droplet impinging on a heated surface". *International Journal of Heat and Mass Transfer*, 51 (19–20), pp. 4728–4742. URL: <http://www.sciencedirect.com/science/article/pii/S001793100800149X> (cited on page 25).

[Sun et al. 2004]

Sun, Y. and C. Beckermann (2004). "Diffuse interface modeling of two-phase flows based on averaging: mass and momentum equations". *Physica D: Nonlinear Phenomena*, 198 (3–4), pp. 281–308. URL: <http://www.sciencedirect.com/science/article/pii/S0167278904003689> (cited on page 23).

[Tan et al. 2007]

Tan, L. and N. Zabaras (2007). "A level set simulation of dendritic solidification of multi-component alloys". *Journal of Computational Physics*, 221 (1), pp. 9–40. URL: <http://www.sciencedirect.com/science/article/pii/S0021999106002737> (cited on page 22).

[Tiller et al. 1953]

Tiller, W. A, K. A Jackson, J. W Rutter, and B Chalmers (1953). “The redistribution of solute atoms during the solidification of metals”. *Acta Metallurgica*, 1 (4), pp. 428–437. URL: <http://www.sciencedirect.com/science/article/pii/0001616053901266> (cited on page 12).

[Tourret et al. 2009]

Tourret, D. and C. A. Gandin (2009). “A generalized segregation model for concurrent dendritic, peritectic and eutectic solidification”. *Acta Materialia*, 57 (7), pp. 2066–2079. URL: <http://www.sciencedirect.com/science/article/pii/S1359645409000184> (cited on page 16).

[Wang et al. 1993]

Wang, C. Y. and C. Beckermann (1993). “A multiphase solute diffusion model for dendritic alloy solidification”. *Metallurgical Transactions A*, 24 (12), pp. 2787–2802. URL: <http://link.springer.com/article/10.1007/BF02659502> (cited on page 16).

[Xu et al. 1991]

Xu, D. and Q. Li (1991). “Gravity- and Solidification-Shrinkage-Induced Liquid Flow in a Horizontally Solidified Alloy Ingot”. *Numerical Heat Transfer, Part A: Applications*, 20 (2), pp. 203–221. URL: <http://dx.doi.org/10.1080/10407789108944817> (cited on page 13).